Characterization and prediction of the discharge coefficient of non-cavitating diesel injection nozzles

José M. Desantes, J. Javier López*, Marcos Carreres, Darío López-Pintor

CMT-Motores Térmicos
Universitat Politècnica de València
Camino de Vera, s/n. 46022 Valencia, SPAIN

Abstract

An experimental and theoretical study about the characterization of the discharge coefficient of diesel injection nozzles under non-cavitating conditions is presented in this paper. A theoretical development based on the boundary layer equations has been performed to define the discharge coefficient of a convergent nozzle. The discharge coefficient has been experimentally obtained for a standard diesel fuel under a wide range of Reynolds numbers by two different techniques: mass flow rate measurements and permeability measurements. Five different nozzles have been used: two multi-hole nozzles that have been tested in the frame of this work, and three other single-hole nozzles, the data of which have been taken from previous studies. The experimental results show good agreement with the theoretical expressions, proving that it is possible to predict the discharge coefficient of a non-cavitating nozzle with the equations shown in this paper.

Keywords: fuel injection, diesel nozzle, discharge coefficient, internal flow

1. Introduction, justification and objective

The increasingly restrictive pollutant emissions regulations applicable to internal combustion engines cause a continuous investigation in different methods

*Corresponding author
Tel: +34 963 879 232. Fax: +34 963 877 659. E-mail: *jolosan3@mot.upv.es*

to reach clean, efficient and marketable engines. Several of the explored methods are focused on the injection system and injection strategy [1], since the way the fuel is delivered by the injection system in modern diesel engines affects not only the performance, but also the noise and the pollutant emissions [2]. A fundamental characteristic of the fuel injection process is the fuel mass flow rate as well as the total amount of fuel injected into the combustion chamber [3]. Therefore, measurement and control of these parameters is one of the most important objectives in engine research and many studies have been carried out to understand the behavior of the flow in the most used nozzle types [4, 5].

The real flow through the nozzle under general operating conditions (where cavitation can be present) is determined by the velocity and density profiles, which are complex and unknown [6]. However, it is possible to characterize this real flow by an effective area, A_{eff}, lower than the geometric one, through which the fluid exits with a uniform effective velocity, u_{eff}, and with a density equal to the one of the liquid fuel, ρ_f; in a way that the simplified flow characterized by these parameters leads to mass and momentum rates equal to the real ones, which can be experimentally measured [7].

The effects of the internal flow on the mass flow rate and momentum flux can be summarized in three different dimensionless coefficients: the velocity coefficient, C_v, the area coefficient, C_a, and the discharge coefficient, C_d [8]. All of them are widely described in Section 3.

Lichtarowicz et al. [9] performed a wide review of discharge coefficient measurements versus the Reynolds number for different nozzles under non-cavitating conditions. A compilation of parametric equations for C_d is shown in that paper. However, all of them are empirical correlations and, therefore, the expressions cannot guarantee their validity out of the range of the experimental measurements. Similar studies have been performed by Kent and Brown [10] and Ohrn et al. [11].

Schmidt and Corradini [12] also published a review about the internal flow of diesel fuel nozzles. Different analytical and multi-dimensional models are shown, focusing on the cavitation behavior. However, cavitation is a phenomenon that normally is avoided in automotive engines and, to this aim, convergent non-cavitating nozzles are usually installed in current engines.

Payri et al. [13] studied the influence of the flow regime on the mass flow rate and momentum flux, and how it affects the spray development in diesel nozzles. Experiments were carried out in three tapered nozzles and spray visualization tests revealed a change in the behavior of the angle and penetration of the spray related to the change of the flow nature. Finally, the authors related these macroscopic parameters to those describing the internal flow (area, velocity and discharge coefficients) and with the geometry of the nozzle. The macroscopic characteristics of direct-injection multi-hole sprays have also been studied by Zeng et al. [14] by using dimensionless analysis, including the discharge coefficient and penetration.

The influence of the injector technology (solenoid or piezoelectric) on the area, velocity and discharge coefficients and on the development of the spray was also studied by Payri et al. in [15, 16]. The authors characterized the hydraulic behavior of different nozzles by means of mass flow rate and momentum flux measurements. It was found that under steady-state conditions, the differences in nozzle geometry dominate on the injector technology. Therefore, the hydraulic characteristics of a nozzle can be studied under steady-state conditions independently of the injector.

Desantes et al. [7] analyzed the flow behavior inside the nozzle for five different nozzles under different injection conditions. The area, velocity and discharge coefficients were obtained under non-cavitating and cavitating conditions and they were related to the spray tip penetration. The authors found that the experimental discharge coefficient decreases when the diameter of the nozzle is increased, probably due to a higher proneness to cavitation.

Vergnes et al. [17] studied the injector nozzles performance (by means of the discharge coefficient) under low-temperature environment conditions. The authors correlated the discharge coefficient with the Reynolds number by an empirical relationship. Therefore, a wide range of experimental data was needed to fit the parameterization of C_d. Moreover, the authors showed the relevance of the discharge coefficient, since the development of the spray (in terms of spray tip penetration) can be deduced from it.

Finally, Dober et al. [18] developed numerical models for investigating the effect of injection hole geometry on the internal nozzle flow, focusing on the injection rate and spray geometry predictions. The authors found that the flow efficiency can be increased up to a 7% by grinding the inlet of the nozzle, proving the high dependence of the maximum discharge coefficient on the inlet geometry.

The main objective of this study is to obtain and validate an alternative theoretical procedure to determine the discharge coefficient of a convergent nozzle under non-cavitating ans steady-state conditions. The study has been done with diesel fuel, but the results can be extrapolated to any other fuel. Despite the fact that the effects of the nozzle geometry on the discharge coefficient are known, most of the correlations available for C_d are mere experimental correlations, obtained by applying a mathematical fitting. An expression that can be used to predict the value of the discharge coefficient avoiding the experimental setup is intended to be defined here. Thus, once the theoretical expressions will be obtained, some experimental results from different nozzles will be used to validate the equations.

Despite the fact that CFD studies can provide a very good approximation to the discharge coefficient of a real nozzle under steady-state conditions, even a simple CFD study needs much more working and computing time than a 0-D correlation like the one presented in this paper. Moreover, the working time needed is highly increased if the hydraulic characterization of the nozzle (variation of C_d with the Reynolds number) wants to be known, hence the interest in developing theoretical 0-D expressions.

It should be noted that realistic conditions can be studied by analyzing the internal flow through a diesel nozzle. It has been proved that the injector needle does not have any effect on the outlet flow when the needle lift has reached around 100 μm, which is a value by far overcome in most real operating conditions, especially during the main injection [19]. Moreover, Salvador et al. [20, 21] have found that the needle effect is negligible under steady-state conditions for several nozzles, under a wide range of conditions and by using different turbulence models. Finally, the set of investigated nozzles is, in some way, random in order to ensure that the resulting expressions can be used with a wide range of nozzles, regardless of their geometry, including the number of holes. Despite the fact that the experimental data have been obtained by using different methodologies, the corresponding parameters of interest in the frame of the present study, derived from the experimental data, have been post-processed in the same way, to ensure they are consistent.

The structure of the paper is as follows: first, the experimental facilities involved in the study are presented. Then, a new expression to describe the discharge coefficient under non-cavitating conditions is theoretically developed. Afterwards, the methodological approach is described, including the experimental methods and the parametric study performed. Next, the predictive methods are validated by comparison with the experiments. Finally, the conclusions of the study are shown.

2. Experimental facilities

The experimental facilities used for the hydraulic characterization of the injection nozzles are the following: hydraulical characterization test rig and injection rate test rig.

2.1. Hydraulical characterization test rig

The objective of the hydraulical characterization test rig (or permeability facility) is to determine the discharge coefficient of an orifice as a function of the pressure drop, or more specifically, the Reynolds number. This characterization can be performed by analysing the continuous flow through the orifice under several conditions of upstream and downstream pressure. To this end, the experimental setup shown in Fig. 1 has been used.

Fuel is pressurized in a commercial common-rail system by a fuel pump electrically driven. Since the fuel is heated during this process, a water heat

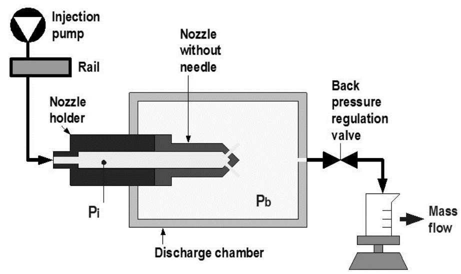

Figure 1: Nozzle hydraulical characterization test rig.

exchanger is used to cool down the flow before it reaches the rail. A manual pressure regulation valve allows the control of the pressure. The nozzle to be characterized is placed, without needle, in a nozzle holder as can be seen in Fig. 1, and a continuous flow from the rail is established. The upstream pressure remains constant thanks to the fuel pump. Fuel flows through the nozzle into a discharge chamber. A backpressure regulation valve allows the manual control of the pressure dowstream the nozzle. Finally, the injected mass is collected into a vessel located on a balance, and the instantaneous fuel rate is measured. The mass flow rate is determined by averaging it during 100 s after a stabilization time. Furthermore, the mean relative deviation of this parameter during the measurement time is lower than 0.5% if $\Delta P < 10$ bar in the nozzle and lower than 0.2% in other cases. Further details about the nozzle hydraulical characterization test rig are given in [22].

The technical characteristics of this facility can be seen in Table 1.

Maximum injection pressure	100	MPa
Back pressure	0.1 - 12	MPa
Minimum cooling temperature	280	K

Table 1: Technical characteristics of the nozzle hydraulical characterization test facility.

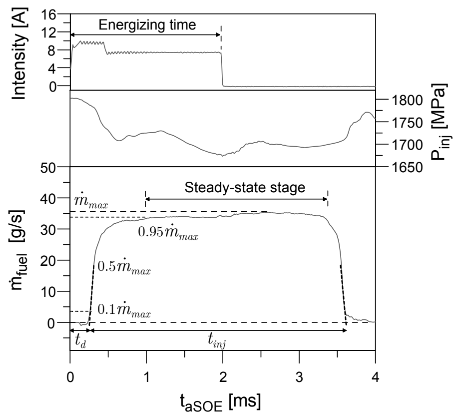

Figure 2: Electrical pulse sent to the injector, evolution of the injection pressure during the process and measured mass flow rate.

2.2. Injection rate test rig

Mass flow rate measurements have been performed in a standard injection rate discharge curve indicator, based on the Bosch method [23]. This installation measures the pressure increment produced by the discharged fuel on a fuel-filled tube, which is directly related to the amount of fuel injected. By this way, information about instantaneous mass flow given by the nozzle along the whole injection process is obtained. The whole system is controlled by a Genotec impulse generator, simulating the operation of the ECU (Electronic Control Unit). More details about this facility can be found in [24]. The discharge coefficient can be measured with this technique by applying energizing times long enough to establish a steady-state fuel rate. The mass flow rate in steady-state conditions is obtained by averaging 50 injections. The coefficient of variation of the mass flow provided by the injector during these 50 injections is lower than 0.3%. Furthermore, two different measurements are performed per condition and the criterion to validate the results is imposing a relative deviation between both lower than 1%. Once the real fuel rate is known, the discharge coefficient can be calculated by comparison with the theoretical one.

Fig. 2 shows a measurement typically obtained with the injection rate test rig. The start of the injection process is defined as the crossing by zero of the line that pass through 50% and 10% of the maximum fuel rate. Thus, the mechanical delay of the injector, t_d, is also defined. An analogous criterion is used to define the closure of the injector and, therefore, the injection time, t_{inj}. Finally, the steady-state stage of the injection event is defined as the time interval in which the mass flow is higher than the 95% of the maximum fuel rate. Thus, the real fuel rate the discharge coefficient is calculated with is obtained by averaging the mass flow in the previous interval.

3. Theoretical description of the discharge coefficient

Three different dimensionless coefficients summarize the effects of the internal flow on the mass flow rate and momentum flux: the velocity coefficient, C_v, the area coefficient, C_a, and the discharge coefficient, C_d.

The velocity coefficient relates the effective velocity to the maximum theoretical velocity, which can be determined by Bernoulli's equation (Eq. 1).

$$u_{th} = \sqrt{\frac{2\Delta P}{\rho_f}} \tag{1}$$

where ΔP represents the difference between the injection pressure (upstream the nozzle) and the back pressure (downstream the nozzle). Thus, the velocity coefficient is defined by Eq. 2:

$$C_v = \frac{u_{eff}}{u_{th}} = \frac{u_{eff}}{\sqrt{\frac{2\Delta P}{\rho_f}}} \tag{2}$$

This coefficient compares the effective velocity with Bernoulli's theoretical velocity, which is achieved if all the pressure energy is transformed into kinetic energy without losses. Thus, this parameter is useful to evaluate the energy losses that occur during the injection process (mainly caused by the changes in cross section) [25]. Therefore, C_v will mainly depend on the nozzle orifice geometry. It should be taken into account that this coefficient summarizes all the energy losses that take place from the point where the injection pressure is measured to the nozzle outlet. So, the losses that belong to the injector itself are considered in the coefficient when a complete injector - nozzle system is analyzed.

The area coefficient characterizes the reduction of the effective area with respect to the geometric one, and is calculated as described in Eq. 3:

$$C_a = \frac{A_{eff}}{A_{geom}} = \frac{A_{eff}}{\frac{\pi}{4}d^2} \tag{3}$$

where d represents the outlet diameter of the nozzle. The area coefficient evaluates the losses of effective cross section due to the existence of a non-uniform velocity profile inside the nozzle, the presence of cavitation zones and the existence of recirculation zones caused by boundary layer separation. Therefore, this coefficient is highly dependant on the Reynolds number of the flow.

Finally, the discharge coefficient is defined as the real measured mass flow rate with respect to the maximum theoretical one. The maximum mass flow rate is evaluated considering a uniform velocity equal to the Bernoulli's theoretical velocity and using the geometric cross-sectional area. Thus, the discharge coefficient can be written as follows:

$$C_d = \frac{\dot{m}}{\dot{m}_{th}} = \frac{A_{eff}u_{eff}\rho_f}{A_{geom}u_{th}\rho_f} = \frac{A_{eff}u_{eff}\sqrt{\rho_f}}{\frac{\pi}{4}d^2\sqrt{2\Delta P}} \tag{4}$$

As can be seen in Eq. 4, the discharge coefficient is equal to the product of the velocity and area coefficients, $C_d = C_v C_a$.

Eventual changes in density and temperature, which are important as injection pressure increases, are taken into account by the previous coefficients, since these changes affect the effective area and velocity. In fact, these coefficients are not constant, but rather functions that depend on the operating conditions.

The discharge coefficient of a convergent nozzle working under non-cavitating and steady-state conditions like the ones that are usually used in automotive direct injection diesel engines is the result of, mainly, two phenomena: the losses caused by the boundary layer separation at the nozzle inlet and the development of a boundary layer on the walls of the nozzle.

The boundary layer separation is caused by the pressure gradients that are originated in the narrowing between the fuel delivery tank (fuel volume upstream the nozzle) and the nozzle. This separation leads to a recirculation zone that reduces the effective fluid passage area, producing a pressure drop that implies a reduction of the effective velocity inside the nozzle. The separation resistance is highly dependent on the boundary layer regime. For a laminar boundary layer this resistance (and the resulting pressure drop) depends only on the geometry, whereas the separation resistance of a turbulent boundary layer increases slightly with increasing Reynolds number [28].

The effects of pressure and viscosity can be decoupled depending on the diameter to length ratio, L/D. Since $L/D < 10$ in a standard diesel nozzle, the boundary layer is not fully developed and two different flows are present: one affected by the boundary layer and another one dominated by pressure effects. The existence of these two flows can be clearly seen in [26], where the radial velocity profile under cavitating and non-cavitating conditions in a nozzle is shown.

Far away from the walls, a uniform inlet flow can be assumed, as could be checked by LES [19] and RANS [20] analysis under similar conditions than the ones assumed in the present work. Thus, the mean velocity through the nozzle, far away from the walls, can be obtained from Bernouilli's equation as follows:

$$\frac{1}{2}u_\infty^2 + \frac{P_{out}}{\rho} = \frac{P_{inj}}{\rho} - \xi\frac{1}{2}u_\infty^2 \tag{5}$$

where $\xi\frac{1}{2}u_\infty^2$ represents the pressure drop (divided by the density of the fluid) caused by the recirculation zone that is generated at the inlet of the nozzle orifices. The coefficient ξ depends on the geometry of the case and can be easily parameterized. In fact, taking into account that the nozzle can be considered as a pipeline connected to a tank with a certain rounding radius at the edges, the coefficient ξ is described by Table 2 [27], where r represents the radius of

r/D	0	0.01	0.02	0.03	0.04	0.05	0.06	0.08	0.12	0.16	≥ 0.2
ξ	0.5	0.43	0.36	0.31	0.26	0.22	0.2	0.15	0.09	0.06	0.03

Table 2: Coefficient ξ of pressure drop at the inlet of the nozzle as a function of the ratio between the radius of rounding and the inlet diameter of the nozzle. Source: [27]

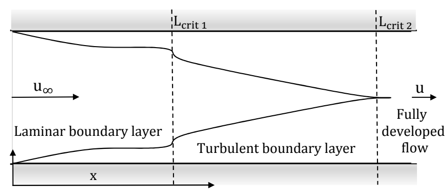

Figure 3: Boundary layer development on the nozzle walls.

rounding and D represents the diameter at the inlet of the nozzle (just at the end of the rounding radius).

The development of a boundary layer on the walls of the nozzle causes a reduction of the effective flow due to the existence of a velocity profile. Fig. 3 shows a scheme of the boundary layer development on the nozzle walls. Taking into account the short lengths of standard automotive nozzles, it can be assumed that $L < L_{crit1}$ and, therefore, that the boundary layer at the nozzle end has a laminar nature. Furthermore, despite the fact that $L_{crit1} < L < L_{crit2}$ can occur at very high Reynolds numbers, the discharge coefficient does not depend on the Re anymore, and its value depends virtually only on the inlet geometry of the nozzle.

It can be demonstrated that the Reynolds number at the outlet of the nozzle is typically lower than the critical Reynolds number and the boundary layer on the walls of the nozzle is under laminar regime. Besides, when the boundary layer becomes turbulent the Reynolds number is high enough and the discharge coefficient can be assumed to be constant with Re. Appendix A shows the theoretical development of a similar model assuming a turbulent boundary layer. The resulting expression for the discharge coefficient is not able to reproduce the experimental results for low Re, which can be assumed as an evidence of the laminar regime in the boundary layer. Of course, turbulence is present in the flow far away from the nozzle walls depending on the Reynolds value. However, an initial laminar boundary layer is developed on the walls and it needs several characteristic lengths to reach the turbulent regime [28] (despite the fact that a turbulent flow is present far away from the walls).

Starting from the Navier-Stokes momentum equation for an incompressible fluid under steady conditions, and taking into account that the axial component parallel to the walls is the predominant one, for the flow far away from the walls the viscous effects are negligible and the pressure gradient for a convergent nozzle can be obtained by combining the continuity equation with the momentum equation (taking the conditions far away from the walls at the orifice outlet as a reference), as follows:

$$\frac{\partial P}{\partial x} = -\rho u_\infty \frac{\partial u_\infty}{\partial x} = -\rho u_\infty u_{\infty out} A_{out} \frac{\partial}{\partial x} \frac{1}{A} \tag{6}$$

where the subscript *out* represents the conditions at the outlet of the nozzle orifice. For the final section of the nozzle this pressure gradient results in:

$$\left.\frac{\partial P}{\partial x}\right._{out} = -\rho u_{\infty out}^2 \frac{2C}{d} \tag{7}$$

where $C = (D - d)/L$ is the conicity of the nozzle and d its outlet diameter.

For the flow that belongs to the boundary layer the viscous effects are dominant and the momentum equation results in:

$$\frac{\partial^2 u}{\partial y^2} = \frac{1}{\mu} \frac{\partial P}{\partial x} \tag{8}$$

where y represents the radial dimension starting from the walls. Eq. 8 can be integrated in the radial dimension with the boundary conditions $[\partial u/\partial y]_{y=\delta} = 0$ and $u_{y=\delta} = u_\infty$, and particularizing for the outlet of the nozzle:

$$u(y)_{out} = u_{\infty out} - \sqrt{2}\frac{\rho u_{\infty out}^2 C}{\mu d}(\delta - y)^2 \tag{9}$$

where δ represents the thickness of the boundary layer.

Therefore, the mass flow rate can be calculated by taking into account the conditions at the outlet of the nozzle. The total outlet flow results as a combination of two: one characterized by an area unaffected by the boundary layer, through which the fluid goes out with a uniform velocity $u_{\infty out}$, which can be obtained from Bernouilli's equation; and another that characterizes the flow through the boundary layer and that can be calculated by integrating the velocity profile $u(y)_{out}$ in the area occupied by such boundary layer. Thus, the total mass flow rate is described by the following equation:

$$\dot{m} = \rho\frac{\pi}{4}d^2 u_{\infty out}\left(1 - \frac{4\sqrt{2}}{3}\frac{\rho u_{\infty out} d}{\mu}C\left(\left(\frac{\delta}{d}\right)^3 - \frac{1}{2}\left(\frac{\delta}{d}\right)^4\right)\right) \tag{10}$$

Finally, from Eq. 1 and Eq. 5, the velocity $u_{\infty out}$ at the nozzle outlet can be related to the maximum theoretical velocity, obtaining:

$$\dot{m} = \rho\frac{\pi}{4}d^2 u_{th}\sqrt{\frac{1}{1+\xi}}\left(1 - \frac{4\sqrt{2}}{3}\frac{\rho u_{th} d}{\mu}\sqrt{\frac{1}{1+\xi}}C\left(\left(\frac{\delta}{d}\right)^3 - \frac{1}{2}\left(\frac{\delta}{d}\right)^4\right)\right) \tag{11}$$

where the discharge coefficient is clearly defined.

Taking into account that the boundary layer through the walls of the nozzle has a laminar nature, the thickness of the boundary layer δ at the outlet section of the nozzle can be scaled with the Reynolds number of the flow as follows [28]:

$$\delta = K\frac{L}{\sqrt{\frac{\rho u_{\infty out} L}{\mu}}} = K\frac{\sqrt{dL}}{\sqrt{\frac{\rho u_{th} d}{\mu}}}(1+\xi)^{1/4} = K\frac{\sqrt{dL}}{\sqrt{Re}}(1+\xi)^{1/4} \tag{12}$$

where the Reynolds number is referred to the outlet diameter, d, and to the theoretical maximum velocity, u_{th}. Besides, K represents the proportionality constant between the thickness of the boundary layer and the Reynolds number referred to the direction of the flow. This constant can be obtained by solving the Karman's equation, e.g. $K \approx 5$ for a flat plate (Blausius' solution) [28], but unfortunately it is not possible to obtain an analytical solution for the problem analyzed in this paper.

Therefore, the final expression for the discharge coefficient derived from Eq. 11 and Eq. 12 is the following:

$$C_d = C_1 - C_2 \left(\frac{1}{\sqrt{Re}} - C_3 \frac{1}{Re} \right) \tag{13}$$

where:

$$C_1 = \sqrt{\frac{1}{1+\xi}} \tag{14}$$

$$C_2 = \frac{4\sqrt{2}}{3} K^3 C \left(\frac{L}{d} \right)^{3/2} (1+\xi)^{-1/4} \tag{15}$$

$$C_3 = \frac{K}{2} \sqrt{\frac{L}{d}} (1+\xi)^{1/4} \tag{16}$$

$$Re = \frac{\rho u_{th} d}{\mu} \tag{17}$$

4. Methodological approach

A parametric study was carried out in the hydraulical characterization test facility and in the injection rate test rig in order to analyze the accuracy of the following new method to characterize discharge coefficients: for a certain nozzle, the discharge coefficient is experimentally obtained with standard diesel fuel under different injection conditions (i.e. as a function of Reynolds). Then, the geometrical aspects of this nozzle are measured by electronic microscopy.

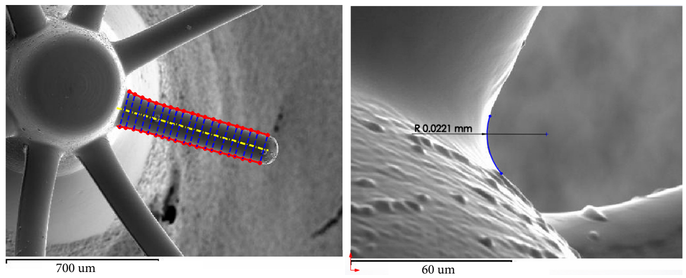

Figure 4: Silicone moulds images. Left.- Bottom view of the whole nozzle. Right.- Detailed view of the inlet radius of rounding.

Afterwards, the discharge coefficient is parameterized with the theoretical expressions previously deducted. Besides, the proportionality constant, K, that appears in the mathematical expressions is adjusted by comparison with the experimental data. Finally, the value of K as a function of the nozzle geometry is obtained and the relative error between the predicted and measured discharge coefficient is calculated. Two multi-hole nozzles has been tested in the frame of this work. Besides, data from three more nozzles (single-hole in this case) have been taken from the literature to further check the validity of the theoretical development.

4.1. Measurements of the nozzle geometry

Silicone has been introduced inside the nozzles, as described in [29], in order to analyse the internal geometrical characteristics of the nozzles used in the current investigation. The silicone moulds have been visualized in a microscope where several pictures of the most relevant geometrical parameters have been taken. By this technique, the following geometrical parameters can be determined [30]: inlet diameter D, outlet diameter d, nozzle length L, inlet rounding of the orifices r and, since they are convergent nozzles, the conicity C. All measurements are taken from two different points of view (side and bottom) and the final dimension is obtained by applying a geometrical average. An example of the microscope images is shown in Fig. 4.

	Holes	d [μm]	$\boldsymbol{D}$ [μm]	$\boldsymbol{L}$ [μm]	$\boldsymbol{r}$ [μm]	$\boldsymbol{C}$	**Source**
Nozzle 1	8	126	150	773	28	0.031	This work
Nozzle 2	8	130	144	563	22	0.024	This work
Nozzle 3	1	156	195	1000	49	0.039	[31]
Nozzle 4	1	138	167	1000	47	0.029	[25]
Nozzle 5	1	112	140	1000	42	0.028	[25]

Table 3: Geometrical parameters of the nozzles used in this work.

	Density [kg/m^3]	**Viscosity [mm^2/s]**	**Surface tension [N/m]**
Standard diesel fuel	825	2.34	0.0205

Table 4: Fuel general properties at 313 K from [33].

The geometrical aspects of the five nozzles used in this paper are summarized in Table 3.

4.2. Measurements of discharge coefficient

Two different types of measurements are involved in this paper. On the one hand, the data that have been taken from previous studies (nozzles 3, 4 and 5) were obtained by mass flow rate measurements. If the real mass flow rate is measured, the discharge coefficient can be directly calculated. A complete description of these methods and of the experimental facilities can be found in [24]. It should be taken into account that the determination of the discharge coefficient by using mass flow rate measurements is affected by the use of an injector. Therefore, the discharge coefficient obtained from these measurements should be decoupled in two: the discharge coefficient of the nozzle and the pressure loss caused by the injector holder (injector body main piece, containing the internal ducts and control orifices if they exist). The pressure loss between the rail and the sac of the injector can be obtained from [32]. Thus, the discharge coefficients taken from [25, 31] are corrected by the pressure drop caused by the injector holder, leading to the discharge coefficients of the nozzles.

$$\rho[kg/m^3] = k1 + k2(T - T_0) + k3(P - P_0) + k4(P - P_0)^2 + k5(T - T0)^2 + k6(P - P_0)(T - T_0)$$

$$a[m/s] = k1 + k2(T - T_0) + k3(P - P_0) + k4(P - P_0)^2 + k5(P - P_0)(T - T_0)$$

$$B[MPa] = k1 + k2(T - T_0) + k3(P - P_0)$$

	k1	**k2**	**k3**	**k4**	**k5**	**k6**
Density, ρ	835.698	-0.6280	0.4914	-0.00070499	0.00073739	0.00103633
Speed of sound, a	1363.05	-3.11349	4.1751	-0.00696763	0.00940137	-
Bulk modulus, B	1581.27	-7.2870	9.4233	-	-	

Table 5: Fuel density (ρ), speed of sound (a) and bulk modulus (B) from [33]. Pressure and temperature have to be used in MPa and K in the correlations, respectively. The reference pressure and temperature are $P_0 = 0.1\ MPa$ and $T_0 = 298\ K$, respectively.

On the other hand, the permeability of nozzles 1 and 2 has been measured in the hydraulical characterization test facility previously described. These experiments allow to obtain directly the discharge coefficient of the nozzle thanks to the absence of the injector needle. The continuous flow through the nozzle is measured for a certain pressure difference at a certain temperature. Finally, the Reynolds number is calculated and the discharge coefficient is obtained by comparison with the maximum theoretical flow. Besides, some measurements of discharge coefficients under high Reynolds numbers have been carried out by mass flow rate measurements due to limitations of maximum pressure in the permeability facility. As it has been said before, standard diesel fuel is used in all the experiments. The physical characteristics of this fuel (evolution of density, viscosity and speed of sound with temperature and pressure) can be found in [33] as $reference\ fuel\ data$. Moreover, a brief summary of the main properties of the fuel can be seen in Tables 4 and 5.

4.3. Parametric study performed

The performed experimental study is described in Table 6. Experimental data have been obtained for a wide range of Reynolds numbers in order to study the asymptotic behavior of the discharge coefficient from very laminar conditions to conditions where C_d is not affected by Re anymore.

	$\boldsymbol{Re}$ **range**	**Measurement**	$\boldsymbol{P_{inj}}$ $[MPa]$	$\boldsymbol{P_{back}}$ $[MPa]$	$\boldsymbol{ET}$ $[\mu s]$	**Source**
Nozzle 1	$1.1 \cdot 10^3$ - $1.3 \cdot 10^4$	Permeability	5 to 60	0.1 to 12	-	This work
Nozzle 1	$2.3 \cdot 10^4$ - $3.3 \cdot 10^4$	Mass flow rate	120 to 220	4.5 to 12	2500	This work
Nozzle 2	$3.7 \cdot 10^3$ - $2.3 \cdot 10^4$	Permeability	10 to 50	0.1 to 6	-	This work
Nozzle 3	$1.8 \cdot 10^3$ - $9.7 \cdot 10^4$	Mass flow rate	30 to 180	2.5 to 5	2500	[31]
Nozzle 4	$6.8 \cdot 10^3$ - $3.7 \cdot 10^4$	Mass flow rate	30 to 150	2.5 to 8	2000	[25]
Nozzle 5	$5.6 \cdot 10^3$ - $3.0 \cdot 10^4$	Mass flow rate	30 to 150	2.5 to 8	2000	[25]

Table 6: Experimental parametric study.

5. Results and discussion

Discharge coefficients obtained by the theoretical Eq. 13 are compared with the experimental results as a method to validate the expression in the studied range. The proportionality constant, K, that appears in the mathematical expressions Eq. 14, 15 and 16, is fitted by comparison with the experimental data. The criterion used to obtain the value of K was minimizing the confidence interval within a level of confidence of 95% of the mean relative error between both experimental and theoretical results.

The value of $K = \delta\sqrt{\frac{\rho u_{\infty out}}{\mu L}}$ as a function of the nozzle geometry can be seen in Fig. 5. The coefficient of determination, R^2, has been calculated and its value can be seen in the figure. $L/d(1-C) \to 0$ results in the flat plate problem, for the Blausius' solution, $K = 4.96$ [28]. A higher value of $L/d(1-C)$ implies higher effects of the walls, where $K \approx 3$ for infinite convergent canal [28]. Thus, it can be expected that the value of K for a conical duct may be lower than the corresponding value for a infinite convergent canal (because of the higher wall effects) and that it may decrease when the relation $L/d(1-C)$ increases. The dependence of K on the geometry of the nozzle can be summarized by Eq. 18.

$$K = 1.838 + 3.122exp\left(-0.310\frac{L}{d(1-C)}\right) \tag{18}$$

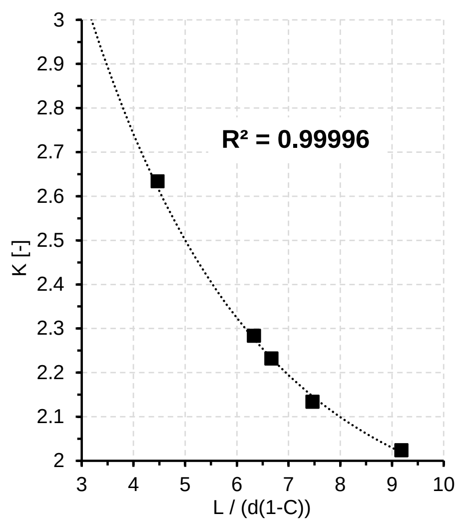

Figure 5: Proportionality constant, K, versus length, diameter and conicity of the nozzle.

whose confidence interval with a level of confidence of 95% of the mean relative error of correlated data is $[0.023, 0.555]\%$.

As already mentioned previously, the values of the discharge coefficients of nozzles 3, 4 and 5 have been obtained by taking into account the pressure drop originated in the injector holder. This pressure drop can be obtained from Fig. 6 as a function of the injection pressure and of the permeability of the nozzle, as explained in [32]. A comparison between the global discharge coefficient (with injector holder) and the discharge coefficient of the nozzle (without injector holder) can be seen in Fig. 7. Of course, the latter C_d is higher than the former.

The comparison between experimental measurements of discharge coefficient and theoretical values obtained by Eq. 13 is plotted in Fig. 8 for the five nozzles. As it can be seen, an excelent agreement between predictions and measurements is achieved. Moreover, the percentage deviation in discharge coefficient (or prediction deviation), ε, was calculated in order to compare the prediction capability of the expression in an easier way. This deviation is defined as follows:

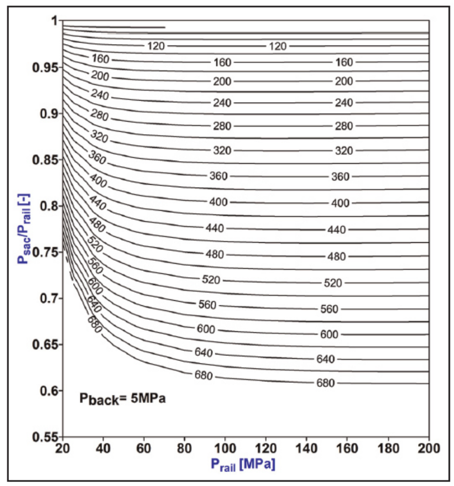

Figure 6: Pressure drop caused by the injector versus injecton pressure for different permeabilities (in [cc/30s]) (source [32]).

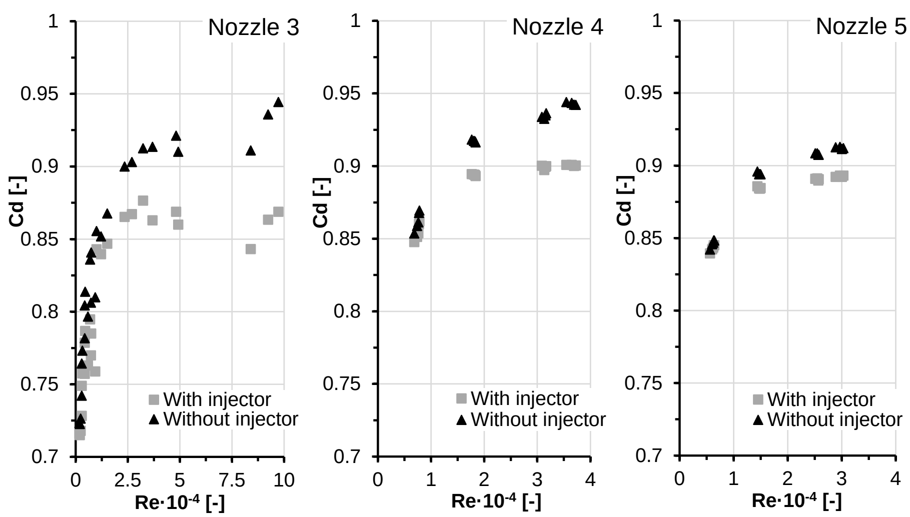

Figure 7: Discharge coefficient of nozzles 3, 4 and 5 with and without injector.

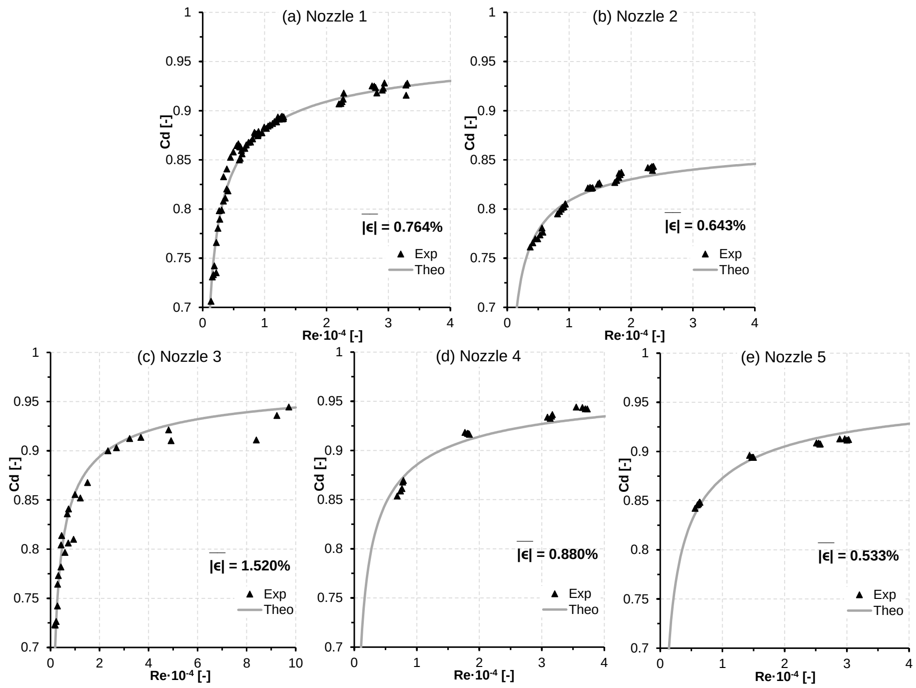

Figure 8: Experimental and theoretical discharge coefficient versus Reynolds number for nozzle 1 (a), nozzle 2 (b), nozzle 3 (c), nozzle 4 (d) and nozzle 5 (e).

$$\varepsilon = \frac{C_{d,th} - C_{d,exp}}{C_{d,exp}} 100 \tag{19}$$

where the subscript th represents a value obtained from the theoretical expression of C_d, whereas the subscript exp represents the corresponding measurement of C_d. The mean relative deviation, $|\bar{\epsilon}|$, has been calculated and its value can be seen in the figure.

Finally, the confidence intervals for the mean relative deviation, $|\bar{\epsilon}|$, with a confidence level of 95% have been calculated for the five nozzles:

- Nozzle 1: $[0.513, 1.014]$ %
- Nozzle 2: $[0.507, 0.764]$ %
- Nozzle 3: $[0.989, 2.052]$ %

- Nozzle 4: $[0.720, 1.041]$ %
- Nozzle 5: $[0.414, 0.652]$ %

As can be deduced from the low values of the confidence intervals of the mean relative deviation, the discharge coefficient of a nozzle under non-cavitating conditions can be obtained from Eq. 13, 14, 15 and 16 with high accuracy. As a final remark, typically, the behavior of the discharge coefficient with the Reynolds number is correlated as follows: $C_d = A - B/\sqrt{Re}$ [34, 35]. This expression is consistent with the theoretical one obtained in this work. Moreover, both expressions should be virtually the same if $C_3/\sqrt{Re} \ll 1$, inequality that is correct, since a typical value of C_3 is ≈ 2.9.

6. Conclusions

In this work a method to predict discharge coefficients of convergent nozzles under non-cavitating conditions is developed. The method is theoretically deducted from the boundary layer equations, and it shows an excelent agreement with the experimental measurements.

The following conclusions can be deduced from this study:

- The discharge coefficient of a nozzle like the ones used in fuel injection systems under non-cavitating conditions can be described by Eq. 13. From a critical $Re_c \approx 10$, the higher the Reynolds number, the higher the discharge coefficient following an asymptotic behavior.
- The asymptote of the discharge coefficient depends only on the geometry of the nozzle inlet. The decreasing rate of C_d for more laminar conditions depends also on geometrical aspects of the nozzle.
- Eq. 14, 15 and 16 can be used to parameterize the discharge coefficient from a theoretical point of view. The comparison with experimental data has shown that C_d can be described by these expressions with high accuracy.

- The low values of the confidence intervals of the mean relative deviation for all nozzles proved that the theoretical expression presented in this work can be used for both single-hole and multi-hole nozzles.

Acknowledgements

The authors would like to thank different members of the CMT-Motores Térmicos team of the Universitat Politècnica de València for their contribution to this work, specially to R. Payri, F.J. Salvador, J. Gimeno and G. Bracho. This work was partly sponsored by "Ministerio de Economía y Competitividad" in the frame of the project "Comprensión de la influencia de combustibles no convencionales en el proceso de inyección y combustión tipo diesel", reference TRA2012-36932. The equipment used in this work has been partially supported by FEDER project funds "Dotación de infraestructuras científico técnicas para el Centro Integral de Mejora Energética y Medioambiental de Sistemas de Transporte (CiMeT), (FEDER-ICTS-2012-06)", in the frame of the operation program of unique scientific and technical infrastructure of the Ministry of Science and Innovation of Spain. This support is gratefully acknowledged by the authors. Finally, the authors would like to thank the Spanish Ministry of Education for financing the PhD. studies of Darío López-Pintor (grant FPU13/02329).

Nomenclature

A_{eff}	Effective area at the outlet of the nozzle
A_{geom}	Geometric area at the outlet of the nozzle
C	Conicity of the nozzle
C_a	Area coefficient
C_d	Discharge coefficient
C_v	Velocity coefficient
d	Outlet diameter of the nozzle
D	Inlet diameter of the nozzle
ET	Energizing time
K	Proportionality constant between the thickness of the boundary layer and the Reynolds number referred to the direction of the flow
L	Nozzle length
P	Pressure

r	Radius of rounding at the inlet of the nozzle
Re	Reynolds number
u	Velocity profile inside the boundary layer
u_{eff}	Effective velocity at the outlet of the nozzle
u_{th}	Theoretical maximum velocity at the outlet of the nozzle
u_{∞}	Velocity outside the boundary layer
x	Axial direction of the nozzle
y	Radial direction of the nozzle
δ	Thickness of the boundary layer
ΔP	Pressure difference between the rail and the outlet of the nozzle
ϵ	Percentage deviation in C_d between experimental and theoretical results
$|\bar{\epsilon}|$	Mean relative deviation between experimental and theoretical results
μ	Viscosity
ξ	Pressure drop coefficient caused by the recirculation zone in the inlet of the nozzle.
ρ	Density

Subscripts

$aSOE$	After start of injection
$back$	Referred to dowstream the nozzle
exp	Referred to experimental results
inj	Referred to injection conditions (in the rail)
out	Referred to the outlet of the nozzle
SOE	Start of injection
th	Referred to theoretical results

Appendix A. Comparison between turbulent and laminar boundary layer

The theoretical development that is shown in Section 3 is performed assuming a laminar boundary layer on the walls of the nozzle. Since there is not any experimental evidence to support this hypothesis, a similar development has been performed assuming a turbulent boundary layer as a method to check what is the regime really present in the boundary layer of the nozzle.

Similarly to the development for a laminar boundary layer, two different flows are assumed: one affected by the boundary layer and another one dominated by pressure effects.

Far away from the walls, a uniform inlet flow can be assumed. Thus, the mean velocity through the nozzle, far away from the walls, can be obtained from Bernouilli's equation as shown by Eq. 5. Starting from the Navier-Stokes momentum equation for an incompressible fluid under steady conditions, and taking into account that the axial component parallel to the walls is the predominant one, for the flow far away from the walls the viscous effects are negligible and the pressure gradient for a convergent nozzle can be obtained by combining the continuity equation with the momentum equation (taking the conditions far away from the walls at the orifice outlet as a reference), resulting in Eq. 6 already shown in the paper.

For the flow that belongs to the boundary layer the viscous effects are dominant. Assuming the Prandtl's mixing length hypothesis as turbulence model, which is a first order and zero equations RANS model, the momentum equation results in:

$$\mu\frac{\partial^2\bar{u}}{\partial y^2} + 2\rho K^2 y\frac{\partial\bar{u}}{\partial y}\frac{\partial\bar{u}}{\partial y} + 2\rho(Ky)^2\frac{\partial\bar{u}}{\partial y}\frac{\partial^2\bar{u}}{\partial y^2} = \frac{\partial P}{\partial x} = -\rho\bar{u}_\infty\frac{\partial\bar{u}_\infty}{\partial x} \tag{A.1}$$

where $\bar{u}$ represents the mean velocity profile in the boundary layer, whereas $\bar{u}_\infty$ represents the mean velocity far away from the walls. K is the Karman's constant, the value of which is $K \approx 0.41$.

On the one hand, the turbulence is negligible in the area of the boundary layer close to the walls (laminar sub-layer). Thus, Eq. A.1 can be integrated with the boundary conditions $\mu[\partial\bar{u}/\partial y]_{y=0} = \tau_w$ and $\bar{u}_{y=0} = \bar{u}_\tau$, where $\tau_w = \rho\bar{u}_\tau^2$ is the wall strain and $\bar{u}_\tau$ is the velocity on the walls, as follows:

$$\bar{u} = -\frac{\rho\bar{u}_\infty}{2\mu}\frac{\partial\bar{u}_\infty}{\partial x}y^2 + \frac{\rho\bar{u}_\tau^2}{\mu}y + \bar{u}_\tau \tag{A.2}$$

On the other hand, the turbulence is dominant in the area far enough from the walls (logarithmic sub-layer). Thus, Eq. A.1 can be integrated with the boundary condition $[\bar{u}]_{y=\delta} = \bar{u}_\infty$ as follows:

$$\bar{u} = \bar{u}_\infty + \frac{\bar{u}_\tau}{K}ln\left(\frac{y}{\delta}\right) \tag{A.3}$$

where δ is the boundary layer thickness.

Assuming that the transition between the laminar and the logarithmic sub-layer occurs at $y \approx \frac{5\mu}{\rho\bar{u}_\tau}$, Eqs. A.2 and A.3 have to match for that particular value of y, since the velocity profile has to be continuous. Thus, an estimator of the velocity on the walls, $\bar{u}_\tau$, can be obtained by imposing Eq. A.2 = Eq. A.3 when $y = \frac{5\mu}{\rho\bar{u}_\tau}$. The natural logarithm of Eq. A.3 can be approximated by truncating its Taylor's series expansion in the second term, and assuming that $\bar{u}_\tau$ is small enough to discard terms of higher order, the following expression is obtained for $\bar{u}_\tau$:

$$\bar{u}_\tau = K\delta^2\frac{\rho\bar{u}_\infty}{\mu}\frac{\partial\bar{u}_\infty}{\partial x} = \frac{2K\delta^2 C}{d}\frac{\rho\bar{u}_\infty^2}{\mu} \tag{A.4}$$

where $\frac{\partial \bar{u}_\infty}{\partial x}$ is calculated as shown by Eq. 9, $C = (D-d)/L$ is the conicity of the nozzle and d its outlet diameter.

Therefore, the mass flow rate can be calculated by taking into account the conditions at the outlet of the nozzle. The total outlet flow results as a combination of two: one characterized by an area unaffected by the boundary layer, through which the fluid goes out with a uniform velocity $\bar{u}_{\infty out}$, which can be obtained from Bernouilli's equation; and another that characterizes the flow through the boundary layer and that can be calculated by integrating the velocity profile $u(\bar{y})_{out}$ in the area occupied by such boundary layer. It should be noted that also two other different areas have to be taken into account in the boundary layer, one that corresponds to the laminar sub-layer and another one that corresponds to the logarithmic sub-layer. Thus, the total mass flow rate is described by the following equation:

$$\begin{aligned}\dot{m} =& \rho\frac{\pi}{4}(d-2\delta)^2\bar{u}_{\infty out}+\\ &+\int_0^{\frac{5\mu}{\rho\bar{u}_\tau}} \pi(\delta-2y)\left(-\frac{\rho\bar{u}_\infty}{2\mu}\frac{\partial\bar{u}_\infty}{\partial x}y^2+\frac{\rho\bar{u}_\tau^2}{\mu}y+\bar{u}_\tau\right)dy+\\ &+\int_{\frac{5\mu}{\rho\bar{u}_\tau}}^{\delta} \pi(\delta-2y)\left(\bar{u}_\infty+\frac{\bar{u}_\tau}{K}ln\left(\frac{y}{\delta}\right)\right)dy\end{aligned} \tag{A.5}$$

From Eq. 1 and Eq. 5, the velocity $\bar{u}_{\infty out}$ at the nozzle outlet can be related to the maximum theoretical velocity, resulting in $\bar{u}_{th} = \bar{u}_{\infty out}\sqrt{1+\xi}$. Assuming that the flow through the laminar sub-layer is much smaller than the flow through the logarithmic sub-layer, and taking into account that the boundary layer through the walls of the nozzle has a turbulent nature, the thickness of the boundary layer δ at the outlet section of the nozzle can be scaled with the Reynolds number of the flow as follows:

$$\delta = K'\frac{L}{\left(\frac{\rho\bar{u}_{\infty out}L}{\mu}\right)^{1/5)}} = K'\frac{d^{1/5}L^{4/5}}{\left(\frac{\rho\bar{u}_{th}d}{\mu}\right)^{1/5}}(1+\xi)^{1/10} = K'\frac{d^{1/5}L^{4/5}}{Re^{1/5}}(1+\xi)^{1/10} \tag{A.6}$$

where the Reynolds number is referred to the outlet diameter, d, and to the theoretical maximum velocity, $\bar{u}_{th}$. Besides, K' represents the proportionality constant between the thickness of the boundary layer and the Reynolds number referred to the direction of the flow. This constant can be obtained by solving the Karman's equation, e.g. $K \approx 5$ for a flat plate (Blausius' solution) [28], but unfortunately it is not possible to obtain an analytical solution for the problem analyzed in this paper.

Thus, the fuel rate delivered by the nozzle is finally defined by the following expression:

$$\dot{m} = \rho\frac{\pi}{4}d^2\bar{u}_{th}\frac{1}{\sqrt{1+\xi}}K_{Cd} \tag{A.7}$$

where the discharge coefficient is defined by $K_{Cd}/\sqrt{1+\xi}$, and $K_{Cd} = f(Re)$ is defined as follows:

$$
\begin{aligned}
K_{Cd} =& 1-\frac{10}{CKK'^2}\left(\frac{d}{L}\right)^{8/5}\frac{(1+\xi)^{8/10}}{Re^{8/5}}+\\
&+\frac{25}{C^2K^2K'^4}\left(\frac{d}{L}\right)^{16/5}\frac{(1+\xi)^{16/10}}{Re^{16/5}}-\\
&-\frac{25}{CK^2K'^2}\left(\frac{d}{L}\right)^{8/5}\frac{(1+\xi)^{13/10}}{Re^{13/5}}+\\
&+\frac{20}{K}\frac{(1+\xi)^{1/2}}{Re}+4CK'^4\left(\frac{L}{d}\right)^{16/5}\frac{Re^{1/5}}{(1+\xi)^{1/10}}-8CK'^3\left(\frac{L}{d}\right)^{12/5}\frac{Re^{2/5}}{(1+\xi)^{1/5}}+\\
&+\left(\frac{50}{CK^2K'^2}\left(\frac{d}{L}\right)^{8/5}\frac{(1+\xi)^{13/10}}{Re^{13/5}}-\frac{20}{K}\frac{(1+\xi)^{1/2}}{Re}\right)ln\left(\frac{5}{2CKK'^3}\left(\frac{d}{L}\right)^{12/5}\frac{(1+\xi)^{7/10}}{Re^{7/5}}\right)
\end{aligned}
\tag{A.8}
$$

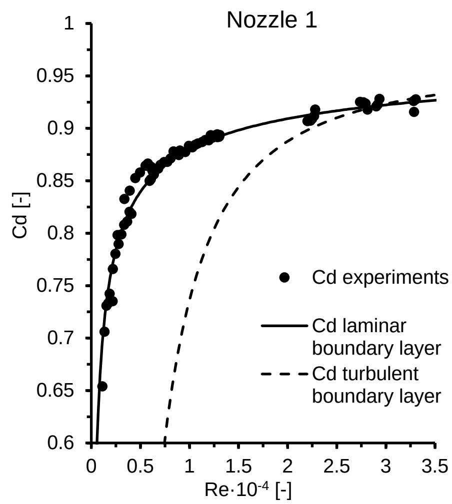

Figure A.9: Experimental and theoretical discharge coefficient versus Reynolds number for nozzle 1. Solid line.- Theoretical expression for C_d assuming laminar boundary layer. Dashed line.- Theoretical expression for C_d assuming turbulent boundary layer.

Fig. A.9 shows the comparison between Eq. 13 and the previous expression to define the discharge coefficient. In Eq. A.8, the value of the proportionality constant K' has been obtained by fitting the values of C_d at high Reynolds numbers, where the assumption of turbulent boundary layer is more robust. As it can be seen, the assumption of turbulent boundary layer leads to a faster diminution of C_d when the Reynolds number decreases, which is an expected result, since the boundary layer thickness of a turbulent boundary layer is higher and, therefore, the flow restrictions are also higher. Since the experimental data cannot be reproduced by an expression deducted from a turbulent boundary layer, the boundary layer has to be in laminar regime in the studied range of Reynolds. It should be noted that for really high Reynolds numbers, where the turbulence is higher, both expressions (laminar and turbulent) trends to coincide, since C_d loses its dependence on Reynolds.

References

[1] F. Payri, A. Broatch, J.M. Salavert, and J. Martín. Investigation of diesel combustion using multiple injection strategies for idling after cold start of passenger-car engines. *Experimental Thermal and Fluid Science*, 34:857–865, 2010.

[2] S.H. Park, S.H. Yoon, and C.S. Lee. Effect of multiple-injection strategies on overall spray behavior, combustion, and emission characteristics of biodiesel fuel. *Applied Energy*, 88:88–98, 2011.

[3] J. Hunicz and P. Kordos. An experimental study of fuel injection strategies in CAI gasoline engine. *Experimental Thermal and Fluid Science*, 35:243–252, 2011.

[4] E. Plamondon and P. Seers. Development of a simplified dynamic model for a piezoelectric injector using multiple injection strategies with biodiesel/diesel-fuel blends. *Applied Energy*, 131:411–424, 2014.

[5] F.J. Salvador, J. Gimeno, J. De la Morena, and M. Carreres. Using one-dimensional modeling to analyze the influence of the use of biodiesels on the dynamic behavior of solenoid-operated injectors in common rail systems: Results of the simulations and discussion. *Energy Conversion and Management*, 54:122–132, 2012.

[6] Z.Y. Sun, X. Li, C. Chen, Y. Yu, and G. Gao. Numerical investigation on effects of nozzle's geometry parameters on the flow and the cavitation characteristics within injector's nozzle for a pressure common-rail DI diesel engine. *Energy Conversion and Management*, 89:843–861, 2015.

[7] F.M. Desantes, R. Payri, J.M. Pastor, and J. Gimeno. Experimental characterization of internal nozzle flow and diesel spray behavior - Part I: Nonevaporative conditions. *Atomization and Sprays*, 15:489–516, 2005.

[8] J. Naber and D. Siebers. Effects of gas density and vaporization on penetration and dispersion of diesel sprays. *SAE International 960034*, 1996.

[9] A.K. Lichtarowicz, R.K. Duggins, and E. Markland. Discharge coefficients for incompressible non-cavitating flow through long orifices. *Journal of Mechanical Engineering Science*, 7:210–219, 1965.

[10] J.C. Kent and G.M. Brown. Nozzle exit flow characteristics for square-edged and rounded inlet geometries. *Combustion Science and Technology*, 30:121–132, 1983.

[11] T.R. Ohrn, D.W. Senser, and A.H. Lefèbvre. Geometrical effects on discharge coefficients for plain-orifice atomizers. *Atomization and Sprays*, 1:137–153, 1991.

[12] D.P. Schmidt and M.L. Corradini. The internal flow of diesel fuel injector nozzles: A review. *International Journal of Engine Research*, 2:1–22, 2001.

[13] R. Payri, F.J. Salvador, J. Gimeno., and R. Novella. Flow regime effects on non-cavitating injection nozzles over spray behavior. *International Journal of Heat and Fluid Flow*, 32:273–284, 2011.

[14] W. Zeng, M. Xu, M. Zhang, Y. Zhang, and D.J. Cleary. Macroscopic characteristics for direct-injection multi-hole sprays using dimensionless analysis. *Experimental Thermal and Fluid Science*, 40:81–92, 2012.

[15] R. Payri, F.J. Salvador, J. Gimeno, and J. De la Morena. Influence of injector technology on injection and combustion development - Part 2: Combustion analysis. *Applied Energy*, 88:1130–1139, 2011.

[16] R. Payri, F.J. Salvador, J. Gimeno, and J. De la Morena. Influence of injector technology on injection and combustion development - Part 1: Hydraulic characterization. *Applied Energy*, 88:1068–1074, 2011.

[17] C. Vergnes, F. Foucher, and R.C. Mounaïm. Discharge coefficient for a diesel injector during cold starting conditions. *Atomization and Sprays*, 19:621–631, 2009.

[18] G. Dober, J. Shi, N. Guerrassi, K. Karimi, and Y. Meslem. Complex physics modelling of diesel injector nozzle flow and spray supported by new experiments. In *8th International Conference on Thermo and Fluid Dynamic Processes in Direct Injection Engines*, Valencia, 2014. THIESEL 2014.

[19] J.M. Desantes, F.J. Salvador, M. Carreres, and J. Martínez-López. Large-eddy simulation analysis of the influence of the needle lift on the cavitation in diesel injector nozzles. *Proceedings of the Institution of Mechanical Engineers*, 229:407–423, 2015.

[20] F.J. Salvador, J. Martínez-López, M. Caballer, and C. De Alfonso. Study of the influence of the needle lift on the internal flow and cavitation phenomenon in diesel injector nozzles by CFD using RANS methods. *Energy Conversion and Management*, 66:246–256, 2013.

[21] F.J. Salvador, M. Carreres, D. Jaramillo, and J. Martínez-López. Comparison of microsac and VCO diesel injector nozzles in terms of internal nozzle flow characteristics. *Energy Conversion and Management*, 103:284–299, 2015.

[22] R. Payri, F.J. Salvador, M. Carreres, and J. De la Morena. Fuel temperature influence on the performance of a last generation common-rail diesel ballistic injector. Part II: 1D model development, validation and analysis. *Energy Conversion and Management*, 114:376–391, 2016.

[23] W. Bosch. The fuel rate indicator: A new measuring instrument for display of the characteristics of individual injection. *SAE Technical Paper 660749*, 1966.

[24] R. Payri, F.J. Salvador, J. Gimeno, and G. Bracho. A new methodology for correcting the signal cumulative phenomenon on injection rate measurements. *Experimental Techniques*, 32:46–49, 2008.

[25] R. Payri, F.J. Salvador, J. Gimeno., and A. García. Flow regime effects over non-cavitating diesel injection nozzles. *Journal of Automobile Engineering*, 226:133–144, 2011.

[26] F. Payri, R. Payri, F.J. Salvador, and J. Martínez-López. A contribution to the understanding of cavitation effects in Diesel injector nozzles through a combined experimental and computational investigation. *Computers and Fluids*, 58:88–101, 2012.

[27] I.E. Idel'cik. *Mémento des pertes de charges*. Eyrolles, 1986.

[28] H. Schlichting and K. Gersten. *Boundary Layer Theory*. Springer, 2000.

[29] V. Macian, V. Bermúdez, R. Payri, and J. Gimeno. New technique for the determination of internal geometry of a diesel nozzle with the use of silicone methodology. *Experimental Techniques*, 27:39–43, 2003.

[30] F. Payri, V. Bermúdez, R. Payri, and F.J. Salvador. The influence of cavitation on the internal flow and the spray characteristics in diesel injection nozzles. *Fuel*, 83:419–431, 2004.

[31] R. Payri, F.J. Salvador, J. Gimeno, and G. Bracho. Understanding diesel injection characteristics in winter conditions. *SAE International 2009-01-0836*, 2009.

[32] J.J. López, F.J. Salvador, O.A. de la Garza, and J. Arrègle. Characterization of the pressure losses in a common rail diesel injector. *Journal of Automobile Engineering*, 226:1697–1706, 2012.

[33] R. Payri, F.J. Salvador, J. Gimeno, and G. Bracho. The effect of temperature and pressure on thermodynamic properties of diesel and biodiesel fuels. *Fuel*, 90:1172–1180, 2011.

[34] R. Payri, J.M. Garcia, F.J. Salvador, and J. Gimeno. Influence of nozzle geometry on spray characteristics in non-evaporating and evaporative conditions. *SAE International 2007-24-0023*, 2007.

[35] F. Payri, V. Bermúdez, R. Payri, and F.J. Salvador. The influence of cavitation on the internal flow and the spray characteristics in diesel injection nozzles. *Fuel*, 83(4):419–431, 2004.